# Design of a BPANN-Adadelta-based speed estimation scheme for a sensorless SCIM

Tista Banerjee
*Inst. of Eng. & Management*
*Univ. of Eng. & Management*
Kolkata, West Bengal, India
tista.banerjee@gmail.com

Sumangal Bhaumik
*Dept of Electrical Engineering*
*Abacus Inst. of Eng. & Management*
Hoogly, West Bengal, India
sumangalstar26@gmail.com

Sudeep Samanta
*Dept of Electrical Engineering*
*MCKV Institute of Eng. & Management*
Howrah, West Bengal, India
sudeep0809@gmail.com

Jinia Dutta
*Dept of Electrical Engineering*
*Abacus Inst. of Eng. & Management*
Hoogly, West Bengal, India
dattajinia@gmail.com

Gourav Saha
*Inst. of Eng. & Management*
*Univ. of Eng. & Management*
Kolkata, West Bengal, India
gourav.saha@uem.edu.in

Jitendranath Bera
*Dept of Applied Physics (EE)*
*University of Calcutta*
Kolkata, West Bengal, India
jnbaphy@caluniv.ac.in

2026 Innovations in Machine, Engineering, and Digital Conference (IMED) | 979-8-3315-6997-6/26/$31.00 ©2026 IEEE | DOI: 10.1109/IMED68921.2026.11484996

***Abstract*—This paper describes an innovative BPANN-based sensorless speed estimation scheme for a voltage source inverter-based squirrel cage induction motor (VSI-SCIM) ASD based on an indirect field-oriented control (IFOC). It is a. The VSI SCIM drive controller is designed such that it precisely estimates speed from equivalent circuit parameter data and d-q axis reactive power during start and running conditions. It also eases the errors in ECP and speed measurement due to the temperature rise of the motor driver. The back-propagation algorithm-based artificial neural network (BPANN) method is used for rapid tuning of the gains of the PI controller and predicting these values under operating mode. For rapid tuning of BPANN, the adadelta rule is used. The simulation result under MATLAB and the prototype model of VSI-SCIM drive controller, with a DSP-based microcontroller, illustrate the efficiency of the suggested algorithm under various operating conditions.**

***Index Terms*—Speed Estimation, Sensorless, IFOC-VSI-SCIM, BPANN, Adadelta, PI Controller**

## I. Introduction

Sensorless vector control of induction motor drive is used to describe the utilization of a vector control scheme on the IM without the need for a speed sensing device [1]. Space vector modulation-based vector control is primarily used in high-end ASD with IM motor drive systems, where accurate rotor position/speed estimation is needed for better dynamic performance as well as efficiency [1]. Inclusion of a shaft-mounted incremental speed sensor (commonly optical encoders) contributes to the cost and sophistication, and degrades the reliability of drive systems. Optical sensors used for speed measurement can provide erroneous results when they are not compatible with the high-speed DSP-based microcontroller, especially when there is continuous variation in speed. As a result, industries are using vector control systems without mechanical speed sensors. More numerous techniques, such as the extended Kalman filter, model reference adaptive systems, slot harmonics, slip estimation method, and auxiliary signal injection, can be used to measure speed [5]–[9].

These complex speed estimation methods are based on variations in motor equivalent circuit parameters. So, an efficient method for the estimation of the ECP is also required for this method to work well [5]–[9].

The temperature fluctuation effect is pronounced in the stator and rotor resistances and will cause inaccurate speed estimation and detune the vector control logic. The temperature fluctuation is caused by environmental change, the presence of harmonics, and overloading, since all change with these [7].

Therefore, temperature compensation of these resistances is necessary. Numerous techniques are suggested, such as dc signal injection, ac signal injection, the Goertzel algorithm to complex current and voltage space vectors, and thermal observers, voltage disturbance observers, etc., to estimate stator resistance or the temperature [7].

These have motivated the proposal of a BPANN-Adadelta-based speed estimation technique to estimate accurately from equivalent circuit parameters and reactive power in the d-q reference frame, without using a sensor [12].

The ECPs are estimated as in [12]–[14]. The proposed method for speed estimation here estimates the speed from the reactive power of the d-q model of the induction method. The PI controller is present in the slip flow path of the dynamic model of the IFOC-based VSI SCIM Drive. These PI controllers are tuned using the BPANN algorithm [2]–[4]. Application of the Adadelta method allows the adjustment of the ANN weight parameters at a faster convergence rate, so that adjusting is performed during motor starting, irrespective of motor capacity [8]–[10]. For the start transient initiation, the nameplate information, voltage, and current feedback signals are employed. For eliminating the effect of temperature fluctuation, the small signal injection technique has been applied as stated in [13]. The performance of the proposed algorithm has been compared with Gradient Descend method and ZN Method. In addition to the above, a machine monitoring unit (MMU) is also implemented that interacts with the DSP-based microcontroller and shows all the machine ECPs, nameplate data, sensed voltage, current, estimated and reference speed, and temperature during stalled and running conditions. The results show that this method can estimate the speed of the IFOC-based SCIM Drive accurately.

## II. Basic Principle for Sensorless Speed Estimation of VSI-SCIM Drive

The IFOC-based controller design is based on the per-phase d-q equivalent circuit of the SCIM, as shown in Fig. 1. The equations that are utilised for the development of the IFOC-based controller are given in (1-4). The reference of stator currents in the d-q axis is derived using equations (1) and (2) [12], [13].

$$\Psi_r = L_m i_{ds}^* \tag{1}$$

$$T_e \triangleq \frac{3}{2}\frac{p}{2}\frac{L_m}{L_r}\Psi_r i_{qs}^*, \quad i_{qs}^* = \frac{T_e G_2}{i_{ds}^*}, \quad G_2 = \frac{4L_m}{3pL_m^2} \tag{2}$$

Where $T_e$ is torque, $\psi_r$ is the flux of the rotor, and $p$ stands for the number of poles. $G_1$ and $G_2$ represent the gains of the flux and torque flow path, respectively. In IFOC, $\psi_{dr} = \psi_r$ and $\psi_{qr} = 0$. The gain $G_3$ is used to generate the slip speed $\omega_{sl}$ according to equation (3), which is further utilized to generate a unit vector of axis transformation according to equation (4).

$$G_3 = \omega_{sl} = \frac{1}{T_r}\frac{i_{qs}^*}{i_{ds}^*}, \quad T_r = \frac{L_r}{R_r} \tag{3}$$

$$\theta_s \triangleq \int \omega_s dt \tag{4}$$

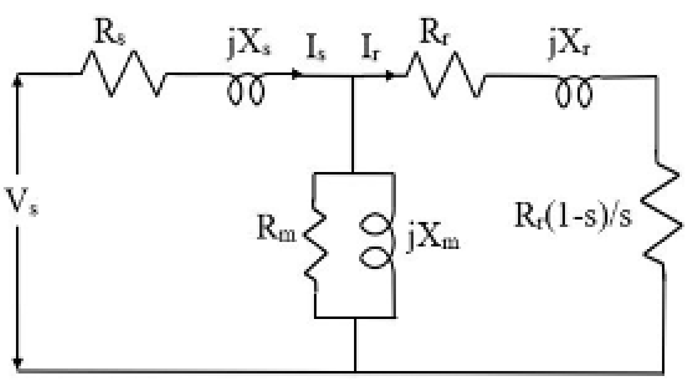


Fig. 1. Per Phase equivalent circuit of an SCIM

Where $R_s$, $R_r$ are the stator and rotor resistances, respectively, and $X_s$ and $X_r$ represent the per-phase inductances. The performance of the IFOC scheme depends upon the ECPs' estimation and calculation of speed. The rotor speed may fluctuate due to fluctuation in load, a change in the time constant because of a temperature rise, as the time constant ($T_r = L_r/R_r$) inversely varies with $R_r$ [12]. A temperature rise tends to increase the stator and rotor copper losses $P_{scl}$, $P_{rcl}$, thus raising the overall loss, $P_{loss}$. Hence, if the supply voltage $V_s$ and the output power ($P_{out}$) remain constant, IM will draw more power from the input, for which the motor efficiency will be reduced, and the stator and rotor currents ($I_s$, $I_r$) will increase [12], [13]. Under steady operating conditions, when the motor starts to accelerate, the $T_e$ becomes maximum at slip $s_m$, as shown in equation (5).

$$\omega_r = \omega_s\left(1 - \frac{s_m T_e}{2T_{em}}\right), \quad s_m = \frac{R_r}{L_s + L_r} \tag{5}$$

At steady state, the d-q axis voltages can be expressed as in equations (6) and (7), at a constant flux.

$$v_{ds}^* = R_s i_{ds}^* - \omega_s \sigma L_s i_{qs}^*, \quad \sigma = 1 - \frac{L_m^2}{L_s L_r} \tag{6}$$

$$v_{qs}^* = R_s i_{qs}^* + \omega_s \sigma L_s i_{ds}^* \tag{7}$$

The reactive power in the d-q axis is expressed as in equation (8)

$$Q_1 = v_{qs} i_{ds} - v_{ds} i_{qs} \tag{8}$$

By substituting the value of $v_{ds}^*$ and $v_{qs}^*$ in equation (8), the reference value of the reactive power is

$$Q_1^* = \omega_s\left(L_s i_{ds}^{*2} + \sigma L_s i_{qs}^{*2}\right) \tag{9}$$

Thus, by comparing equations (8) and (9), we get

$$\omega_s = \frac{v_{qs} i_{ds} - v_{ds} i_{qs}}{L_s i_{ds}^{*2} + \sigma L_s i_{qs}^*} \tag{10}$$

Accordingly, the shaft speed is estimated by

$$\omega_r = \omega_s - \omega_{sl}, \quad \omega_{sl} = \left(K_{psl} + \frac{K_{isl}}{s}\right)(G_3^* - G_3) \tag{11}$$

The $\omega_{sl}^*$ can be estimated from the $i_{qs}^*$ and $i_{ds}^*$, and $\omega_{sl}$ can be estimated from $i_{qs}$ and $i_{ds}$. Hence, $G_3^*$ and $G_3$ are evaluated.

To guarantee correct estimation of the $\omega_{sl}$, a $PI_{sl}$ controller of gain $k_{p\omega sl}$, $k_{i\omega sl}$ is proposed as in equation (11). The schematic of the speed estimation process is depicted in Fig. 2. The PI controller in this case is also trained with the BPANN algorithm. For precise estimation of speed, estimating the ECPs before start and also in running condition is also necessary, which has been fully discussed in [12], [13]. The PI controller has been tuned with Gradient Descend method (GD) first. Since GD method does not have capability to adapt the learning rate so it could not provide satisfactory result which was efficiently achieved by adadelta method.

## III. Calculation of the $K_{psl}$ and $K_{isl}$ using BPANN

The equation of PI controller is shown in equation (12)

$$u(t) = K_p e(t) + K_i \int e(t)dt \tag{12}$$

Where the error between the slips is $e(t)$, $K_p$ and $K_i$ are the gain parameters of the controller, which need to be tuned. For the design of a BPANN-based PI Controller, the above structure has been utilized. For gain tuning, the FOPDT so chosen is of 1st order as

$$G(s) = \frac{K}{T_r s + 1} e^{-Ds} \tag{13}$$

where $K$ = process gain, $\tau$ = time constant, $D$ = delay. For implementing it in BPANN, the following architecture has been used for each gain parameter:

TABLE I
BPANN Architecture

| Parameter | Value/Type |
|---|---|
| Input | Three neurons |
| Output | Two neurons |
| 1st Hidden Layer | Four neurons |
| 2nd Hidden Layer | Two neurons |
| Training algorithm | Adadelta for faster convergence |
| Activation Function | Leaky Relu |
| Total time taken | 140$\mu$s |

The difference between $G_3^*$ and $G_3$ is considered as the error '$e_j$'. The inputs jth neurons are mapped to every neuron of the 1st hidden layer by their respective weights $w_{nj}$, which have been randomly chosen for where $n$ represents the number of weights. The neuron of the 1st hidden layer is expressed as in equation (14):

$$\begin{bmatrix} h_{11j} \\ h_{12j} \\ h_{13j} \\ h_{14j} \end{bmatrix} = \begin{bmatrix} w_{1j} & w_{2j} & w_{3j} \\ w_{4j} & w_{5j} & w_{6j} \\ w_{7j} & w_{8j} & w_{9j} \\ w_{10j} & w_{11j} & w_{12j} \end{bmatrix} \begin{bmatrix} e_{j1} \\ e_{j2} \\ e_{j3} \end{bmatrix} \tag{14}$$

Similarly, for the 2nd layer:

$$\begin{bmatrix} h_{21j} \\ h_{22j} \end{bmatrix} = \begin{bmatrix} w_{13j} & w_{14j} & w_{15j} & w_{16j} \\ w_{17j} & w_{18j} & w_{19j} & w_{20j} \end{bmatrix} \begin{bmatrix} s_{11j} \\ s_{12j} \\ s_{13j} \\ s_{14j} \end{bmatrix} \tag{15}$$

This BPANN architecture minimized the vanishing gradient and exploding gradient problems. Its performance also depends upon the appropriate choice of the activation function, loss function, learning rate ($\eta$), and optimization algorithm. Hence the activation function Leaky Relu is used, mathematically formulated as:

$$f(x) = \begin{cases} x & x > 0 \\ 0.01x & x \leq 0 \end{cases} \tag{16}$$

Adadelta optimization algorithm is chosen for faster convergence as weight updation method [12]–[14]. If learning rate $\eta$ is too small, the convergence time will become large, whereas for large $\eta$, it can retard convergence, which can lead to oscillations around the minima or could diverge, which has been overcome by the selection Adadelta method. The outputs $[K_{pslj}, K_{islj}]$ are evaluated using equation (17):

$$\begin{bmatrix} K_{pslj} \\ K_{islj} \end{bmatrix} = \frac{1}{2} \begin{bmatrix} w_{21j} & w_{22j} \end{bmatrix} \begin{bmatrix} s_{21j} \\ s_{22j} \end{bmatrix} \tag{17}$$

$$w_{n+1} = w_n - \frac{\eta}{\sqrt{\varepsilon + r_n}} g_n, \quad r_n = \sum_{\tau=1}^{n} g_\tau^2, \quad g_n = \frac{\partial E}{\partial w_n} \tag{18}$$

Where $r_n$ is the sum of the squared terms of the gradients $g_\tau$. Here, the $\eta$ declines sharply, and it will also reach zero [12], [13]. Thus, to eliminate this, a window size $wd$ is given for squared gradient terms, and this variant of Adagrad is referred to as Adadelta. The equation (18) is therefore altered as:

$$w_{n+1} = w_n - \frac{\eta}{\sqrt{\gamma + r_n^{wd}}} g_n \tag{19}$$

The value of $r_n$ can be expressed as:

$$r_n = \sum_{\tau=1}^{n} \sum_{\tau=1}^{wd} p g_\tau^2, \quad p = (\tau - w_d) = 1, \ p \geq 1, \ p = 0 \tag{20}$$

Therefore, adadelta is a refined version of the adagrad algorithm that eliminates its biggest drawbacks. Therefore, this algorithm is applied in comparing the $K_{psl}$ and $K_{isl}$ values initially, and they are updated while executing the conditions. Loss or error functions $E$ for each of the jth parameters is depicted in equation (21), which are minimized by applying the adadelta rule. The weights are recalculated in a back propagation approach:

$$E = \frac{1}{N} \sum \left\{ (K_{pslj} - K_{pslt})^2 + (K_{islj} - K_{islt})^2 \right\} \tag{21}$$

Initially, the values obtained for the Z-N Methods are used as target values. Once the BPANN model is tuned, it becomes capable enough to predict the output.

## IV. Results

The feasibility of the controller design as proposed by the Adadelta algorithm is tested in two stages: (i) initially, the complete speed estimation scheme is simulated in the MATLAB/Simulink environment. (ii) Then the scheme is realized in a prototype system of VSI-SCIM drive with a graphical user interface for parameter observation tasks referred to as Machine monitoring unit (MMU). For the development of the hardware, a digital signal processor (DSP) compatible microcontroller (DSPIC30F4011) is used, which is based on cutting-edge hardware capable of processing information at 30 MIPS, as indicated in Fig. 4.

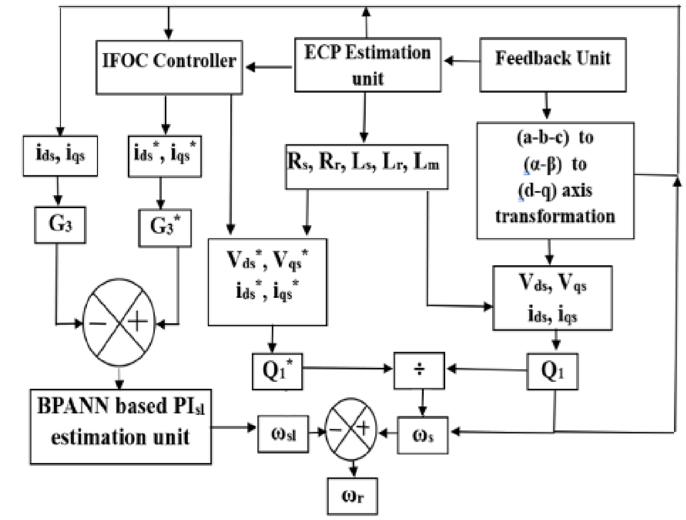


Fig. 2. Schematic of the proposed Speed Estimation Scheme

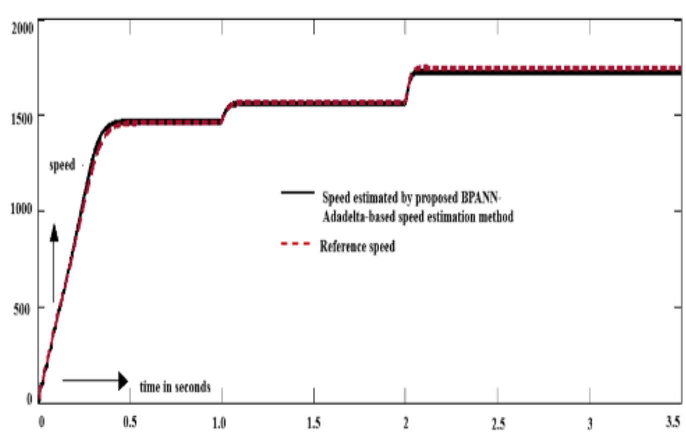


Fig. 3. Speed response of 3.7 kW SCIM. Estimation of speed by the proposed sensorless scheme, even when the speed varies.

The required power modules of IGBT and driver circuits are used to supply the regulated input voltage to the motor. The SVM trigger pulses required are taken from the DSPIC controller, which runs at a frequency of 10 kHz to generate the specified voltage and frequency [12]–[14]. The firmware is coded in a way such that it can make all the measurements, calculate errors, and take required corrections as and when required to produce the desired SVM signals according to the algorithm proposed. The SVM duty cycles are then set in the subsequent cycle, at 200 $\mu$s. The firmware also sends all the data that is analyzed to a PC through its serial communication at 76.8 kbps to the MMU [12]–[14]. It also sends back feedback signals from the Hall voltage, Hall current, optical speed, and temperature feedback units, etc. The demand speed and name plate data are received by the microcontroller from the MMU.

The estimated speed is provided for a broad range of reference speeds in Table IV. The above is confirmed by using the speed estimated by an optical sensor that is fixed on the rotor shaft of the motor. The sensored and sensorless control percentage error is calculated, and it is confirmed that the sensorless control can be used equally to estimate the speed. Fig. 3 illustrates that the proposed method's speed estimation is consistent with the reference speed even when the speed is of a varying nature. The PI controllers are first tuned using the Z-N Method and GD method, and subsequently trained using the BPANN-Adadelta method.

The value of the tuned gain parameters has been tabulated in Table II. The variation of speed has been shown in Table III with the variation of rotor resistance which has varied with temperature. It also shows that the modulation index of the SVM-based pulse with the modulation scheme also changes.

## V. Conclusion

This work presents the design of speed sensorless induction motor drive controller to estimate speed without using a speed sensor. Adadelta-based BPANN Algorithm is used for estimation of PI Controller gain parameters. It has been seen from Table II that time response has been improved with PI controller gain parameters estimated by using BPANN adadelta-based technique. It has been seen from Table IV that the speed estimated in real-time is very accurate. Table III also reflects that transient response criteria changes with the change of $R_r$ with temperature. Fig 3 demonstrates that speed estimated using the $PI_{sl}$ estimated by BPANN algorithm tracks the desired speed as well as changes as per it. Hence, it can be asserted that speed estimation is accurate in running mode, and the IFOC logic will not get detuned. Hence, this approach can be adopted for estimation in running conditions.

Future research may extend the BPANN–Adadelta-based speed estimation framework by incorporating hybrid optimiza-

TABLE II
Transient response of PI Controller gain tuning done initially with Z-N Method and then with the proposed scheme after training

| Method | Kp | Ki | Mp | Tp | Ts |
|---|---|---|---|---|---|
| Z-N | 10.27 | 36.35 | 30 | 0.1 | 0.2 |
| BPANN-based Gradient-Descend | 10.28 | 23.42 | 10.65 | 0.1 | 0.174 |
| BPANN-based proposed method | 10.23 | 10.21 | 4.62 | 0.1 | 0.12 |

TABLE III
Effect of Rr Change on speed as rotor resistance change with Temperature

| T | Rr | Ls | $\tau_r$ | $\omega_r$ | Nr | M |
|---|---|---|---|---|---|---|
| T+10 | 1.84 | 0.1702 | 0.09239 | 147.0462 | 1404.9 | 0.8 |
| T+20 | 1.91 | 0.1702 | 0.0894 | 146.711 | 1401.7 | 0.811 |
| T+30 | 1.98 | 0.1702 | 0.0879 | 146.507 | 1339.75 | 0.824 |
| T+40 | 2.01 | 0.1702 | 0.0865 | 146.314 | 1397.91 | 0.827 |

TABLE IV
ESTIMATION OF SPEED WITH THE PROPOSED SENSORLESS SCHEME

| Demand Speed (Nr*) in rpm | Speed Estimated Using Proposed BPANN Method (Nr1) in rpm | Speed evaluated by Optical sensor(Nr2) in rpm | %Error (Nr-Nr1) | %Error (Nr-Nr2) |
|---|---|---|---|---|
| 400 | 399.86 | 400 | 0.035 | 0 |
| 600 | 600.2 | 601 | -0.033 | 0.1 |
| 800 | 799.71 | 800 | 0.03 | 0 |
| 1000 | 1000.2 | 1000 | 0.02 | 0 |
| 1200 | 1199.5 | 1201 | 0.041 | 0.1 |
| 1400 | 1400.3 | 1400 | -0.02 | 0 |

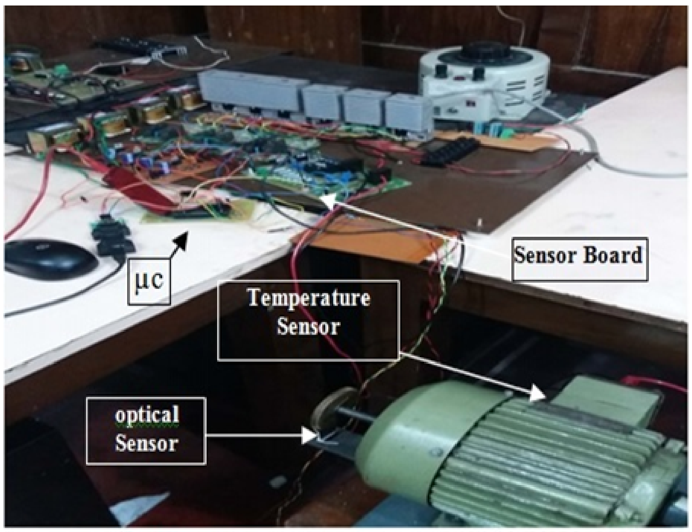


Fig. 4. Prototype model of 3.7 kW IFOC-based VSI SCIM.

tion and ensemble learning strategies to enhance convergence speed and estimation robustness. Inspired by intelligent optimization methodologies presented in [15] and [16], adaptive hyperparameter tuning and hybrid metaheuristic–gradient learning mechanisms could be integrated to improve sensorless SCIM speed estimation accuracy under parameter variations and load disturbances. Such intelligent augmentation may strengthen real-time stability and generalization performance in practical drive systems.

## REFERENCES

[1] Bose, B. K. (2002). Modern power electronics and AC drives. Prentice Hall. Inc, Publication, 70-74.

[2] Ang, K. H., Chong, G., & Li, Y. (2005). PID control system analysis, design, and technology. IEEE transactions on control systems technology, 13(4), 559-576.

[3] Tzafestas, S., & Kapsiotis, G. (1994). PID self-tuning control combining pole-placement and parameter optimization features. Mathematics and computers in simulation, 37(2-3), 133-142.

[4] Banerjee, T., Chowdhuri, S., Sarkar, G. and Bera, J., 2012. Performance comparison between GA and PSO for optimization of PI and PID controller of direct FOC induction motor drive. International Journal of Scientific and Research Publications, 2(7), pp.1-8.

[5] Chen, J., Huang, J., and Sun, Y. (2019). Resistance and speed estimation in sensorless induction motor drives using a model with known regressors. IEEE Transactions on Industrial Electronics, 66(4), 2659–2667.

[6] Zaky, M. S., Metwaly, M. K., Azazi, H. Z., and Deraz, S. A. (2018). A new adaptive SMO for speed estimation of sensorless induction motor drives at zero and very low frequencies. IEEE Transactions on Industrial Electronics, 65(9), 6901-6911.

[7] Zhi Gao, Habetler, T. G., and Harley, R. G. (2009). A complex space vector approach to rotor temperature estimation for line-connected induction machines with impaired cooling. IEEE Transactions on Industrial Electronics, 56(1), 239–247.

[8] Tang, J., Yang, Y., Blaabjerg, F., Chen, J., Diao, L., and Liu, Z. (2018). Parameter identification of inverter-fed induction motors: A review. Energies, 11(9), 2194.

[9] Chandra, B. M., Prasantlr, B. V., and Manindher, K. G. (2018). A review on parameter estimation techniques in decoupling control of induction motor drive. 2018 4th International Conference on Electrical Energy Systems (ICEES).Chennai, India, 7-9 Feb. 2018. doi:10.1109/icees.2018.8443209

[10] Panchal, F. S., & Panchal, M. (2014). Review on methods of selecting number of hidden nodes in artificial neural network. International Journal of Computer Science and Mobile Computing, 3(11), 455-464.

[11] Wang, H., Ge, X., Yue, Y., and Liu, Y.-C. (2020). Dual phase-locked loop-based speed estimation scheme for sensorless vector control of linear induction motor drives. IEEE Transactions on Industrial Electronics, 67(7), 5900–5912.

[12] Banerjee, T., Bera, J.N. Adadelta-Based BPANN Controller for Online Equivalent Parameter Estimation of Squirrel Cage Induction Motor Drive. Trans Indian Natl. Acad. Eng. 7, 1291–1310 (2022). https://doi.org/10.1007/s41403-022-00363-x

[13] Banerjee, T., Bera, J.N. Online equivalent parameter estimation using BPANN controller with low-frequency signal injection for a sensorless induction motor drive. Journal of Electrical Systems and Inf Technol 9, 20 (2022). https://doi.org/10.1186/s43067-022-00060-3

[14] Banerjee, T., Bera, J.N. An Improved Torque Ripple Reduction Controller for Smooth Operation of Induction Motor Drive. J Control Autom Electr Syst 34, 247–264 (2023). https://doi.org/10.1007/s40313-022-00945-8

[15] D. Arockiam, A. Abdullah, and V. Raju, "Intelligent Crop Disease Detection and Classification Using Deep Convolution Neural Network with Honey Badger Algorithm on Image Data," *Journal of Intelligent Systems and Internet of Things*, vol. 14, no. 2, pp. 178–188, 2025, doi: 10.54216/JISIoT.140215.

[16] D. Arockiam, A. Abdullah, and V. Raju, "Robustness of Ensemble Deep Learning Model with Zebra Optimization Algorithm for Weather-Related Disaster Detection System Using Remote Sensing Images," *Fusion: Practice and Applications*, vol. 19, no. 1, pp. 222–234, 2025, doi: 10.54216/FPA.190117.